

**Western blotting**

Ribosomal complexes assembled and purified as described above were TCA-precipitated. Proteins were resolved on 12% polyacrylamide gel, transferred to nitrocellulose membrane and probed for eIF1 and eIF5B using T7-tag antibodies (Novagen) and for eIF2 $\alpha$  and eIF3 (p170) using specific antibodies.

Received 13 September; accepted 16 November 1999.

1. Merrick, W. C. Mechanism and regulation of eukaryotic protein synthesis. *Microbiol. Rev.* **56**, 291–315 (1992).
2. Pestova, T. V., Borukhov, S. I. & Hellen, C. U. T. Eukaryotic ribosomes require initiation factors 1 and 1A to locate initiation codons. *Nature* **394**, 854–859 (1998).
3. Chakrabarti, A. & Maitra, U. Functions of eukaryotic initiation factor 5 in the formation of an 80S ribosomal polypeptide chain initiation complex. *J. Biol. Chem.* **266**, 14039–14045 (1991).
4. Das, K., Chesevich, J. & Maitra, U. Molecular cloning and expression of cDNA for mammalian translation initiation factor 5. *Proc. Natl Acad. Sci. USA* **90**, 3058–3062 (1993).
5. Huang, H.-K., Yoon, H., Hannig, E. M. & Donahue, T. F. GTP hydrolysis controls stringent selection of the AUG start codon during translation initiation in *Saccharomyces cerevisiae*. *Genes Dev.* **11**, 2396–2413 (1997).
6. Choi, S. K., Lee, J. H., Zoll, W. L., Merrick, W. C. & Dever, T. E. Promotion of Met-tRNA<sup>Met</sup> binding to ribosomes by yIF2, a bacterial IF2 homolog in yeast. *Science* **280**, 1757–1760 (1998).
7. Lee, J. H., Choi, S. K., Roll-Mecak, A., Burley, S. K. & Dever, T. E. Universal conservation in translation initiation revealed by human and archaeal homologs of bacterial translation factor IF2. *Proc. Natl Acad. Sci. USA* **96**, 4342–4347 (1999).
8. Sacerdot, C., Dessen, P., Hershey, J. W. B., Plumbridge, J. A. & Grunberg-Manago, M. Sequence of the initiation factor IF2 gene; unusual protein features and homologies with elongation factors. *Proc. Natl Acad. Sci. USA* **81**, 7787–7791 (1984).
9. Kolakofsky, D., Dewey, K. F., Hershey, J. W. B. & Thach, R. E. Guanosine 5'-triphosphatase activity of initiation factor 2. *Proc. Natl Acad. Sci. USA* **61**, 1066–1070 (1968).
10. Godefroy-Colburn, T. et al. Light-scattering studies showing the effect of initiation factors on the reversible dissociation of *Escherichia coli* ribosomes. *J. Mol. Biol.* **94**, 461–478 (1975).
11. Luchin, S. et al. *In vitro* study of two dominant inhibitory GTPase mutants of *Escherichia coli* translation initiation factor IF2. Direct evidence that GTP hydrolysis is necessary for factor recycling. *J. Biol. Chem.* **274**, 6074–6079 (1999).
12. Lockwood, A. H., Sarkar, P. & Maitra, U. Release of polypeptide chain initiation factor IF-2 during initiation complex formation. *Proc. Natl Acad. Sci. USA* **69**, 3602–3605 (1972).
13. Merrick, W. C., Kemper, W. M. & Anderson, W. E. Purification and characterization of homogenous initiation factor M2A from rabbit reticulocytes. *J. Biol. Chem.* **250**, 5556–5562 (1975).
14. Trachsel, H., Emi, B., Schreier, M. H. & Staehelin, T. Initiation of mammalian protein synthesis. II. The assembly of the initiation complex with purified initiation factors. *J. Mol. Biol.* **116**, 755–767 (1977).
15. Benne, R., Brown-Luedi, M. L. & Hershey, J. W. B. Purification and characterization of protein synthesis initiation factors eIF-1, eIF-4C, eIF-4D, and eIF-5 from rabbit reticulocytes. *J. Biol. Chem.* **253**, 3070–3077 (1978).
16. Peterson, D. T., Safer, B. & Merrick, W. C. Role of eukaryotic initiation factor 5 in the formation of 80S initiation complexes. *J. Biol. Chem.* **254**, 7730–7735 (1979).
17. Pestova, T. V., Shatsky, I. N., Fletcher, S. P., Jackson, R. J. & Hellen, C. U. T. A prokaryotic-like mode of binding of cytoplasmic eukaryotic ribosomes to the initiation codon during internal initiation of translation of Hepatitis C and Classical Swine fever virus RNAs. *Genes Dev.* **12**, 67–83 (1998).

**Acknowledgements**

We thank W. Merrick for discussions, D. Etchison and R. Schneider for antibodies, and L. Siconolfi-Baez for sequencing eIF5B. These studies were supported by grants from the NIH to C.U.T.H. and T.V.P.

Correspondence and requests for materials should be addressed to T.V.P. (e-mail: tpestova@netmail.hscbklyn.edu).

**A synthetic oscillatory network of transcriptional regulators**

**Michael B. Elowitz & Stanislas Leibler**

*Departments of Molecular Biology and Physics, Princeton University, Princeton, New Jersey 08544, USA*

Networks of interacting biomolecules carry out many essential functions in living cells<sup>1</sup>, but the ‘design principles’ underlying the functioning of such intracellular networks remain poorly understood, despite intensive efforts including quantitative analysis of relatively simple systems<sup>2</sup>. Here we present a complementary approach to this problem: the design and construction of a synthetic network to implement a particular function. We used three transcriptional repressor systems that are not part of any natural biological clock<sup>3–5</sup> to build an oscillating network, termed

the repressilator, in *Escherichia coli*. The network periodically induces the synthesis of green fluorescent protein as a readout of its state in individual cells. The resulting oscillations, with typical periods of hours, are slower than the cell-division cycle, so the state of the oscillator has to be transmitted from generation to generation. This artificial clock displays noisy behaviour, possibly because of stochastic fluctuations of its components. Such ‘rational network design’ may lead both to the engineering of new cellular behaviours and to an improved understanding of naturally occurring networks.

In the network shown in Fig. 1a, the first repressor protein, LacI from *E. coli*, inhibits the transcription of the second repressor gene, *tetR* from the tetracycline-resistance transposon Tn10, whose protein product in turn inhibits the expression of a third gene, *cI* from  $\lambda$  phage. Finally, CI inhibits *lacI* expression, completing the cycle. That such a negative feedback loop can lead to temporal oscillations in the concentrations of each of its components can be seen from a simple model of transcriptional regulation, which we used to design the repressilator and study its possible behaviours (Box 1). In this model, the action of the network depends on several factors, including the dependence of transcription rate on repressor concentration, the translation rate, and the decay rates of the protein and messenger RNA. Depending on the values of these parameters, at least two types of solutions are possible: the system may converge toward a stable steady state, or the steady state may become unstable, leading to sustained limit-cycle oscillations (Fig. 1b, c).

We found that oscillations are favoured by strong promoters coupled to efficient ribosome-binding sites, tight transcriptional repression (low ‘leakiness’), cooperative repression characteristics, and comparable protein and mRNA decay rates (Box 1, Fig. 1b). A general obstacle to the design of biochemical networks is uncertainty about the values of parameters that characterize the interactions between different components. In our network, estimates of the order of magnitude of the relevant parameters seem to be compatible with the possibility of oscillations. Nevertheless, to increase the chances that the artificial network would function in the oscillatory regime, we made two alterations to natural components. First, to address transcriptional strength and tightness, we used strong, yet tightly repressible hybrid promoters, developed previously, which combine the  $\lambda$  P<sub>L</sub> promoter with *lac* and *tet* operator sequences<sup>6</sup>. Second, to bring the effective repressor protein lifetimes closer to that of mRNA (about 2 min, on average, in *E. coli*<sup>7</sup>), we inserted a carboxy-terminal tag, based on the *ssrA* RNA sequence<sup>8</sup>, at the 3’ end of each repressor gene. Proteases in *E. coli* recognize this tag and target the attached protein for destruction<sup>9,10</sup>. Such tags have been shown to reduce the half-life of the  $\lambda$  repressor DNA-binding domain from more than 60 min to around 4 min (ref. 8) and diminish the half-life of green fluorescent protein (GFP) to about 30–40 min (ref. 11).

With these considerations in mind, we used standard molecular biology techniques to construct a low-copy plasmid encoding the repressilator and a compatible, higher-copy reporter plasmid containing the tet-repressible promoter P<sub>tetO1</sub> (ref. 6) fused to an intermediate stability variant of *gfp*<sup>11</sup> (Fig. 1a). Because the inducer IPTG interferes with repression by LacI, we expected that a transient pulse of IPTG might be capable of synchronizing a population of repressilator-containing cells. A culture of *E. coli* MC4100 containing the two plasmids and grown in media containing IPTG displayed what appeared to be a single damped oscillation of GFP fluorescence per cell after transfer to media lacking IPTG (results not shown). Because individual cells have no apparent means of maintaining synchronization, we studied the repressilator by isolating single cells under the microscope and monitoring their fluorescence intensity as they grew into small two-dimensional microcolonies consisting of hundreds of progeny cells. In these experiments, total observation time was limited by the colony entering a stationary phase after about 10 hours of growth at

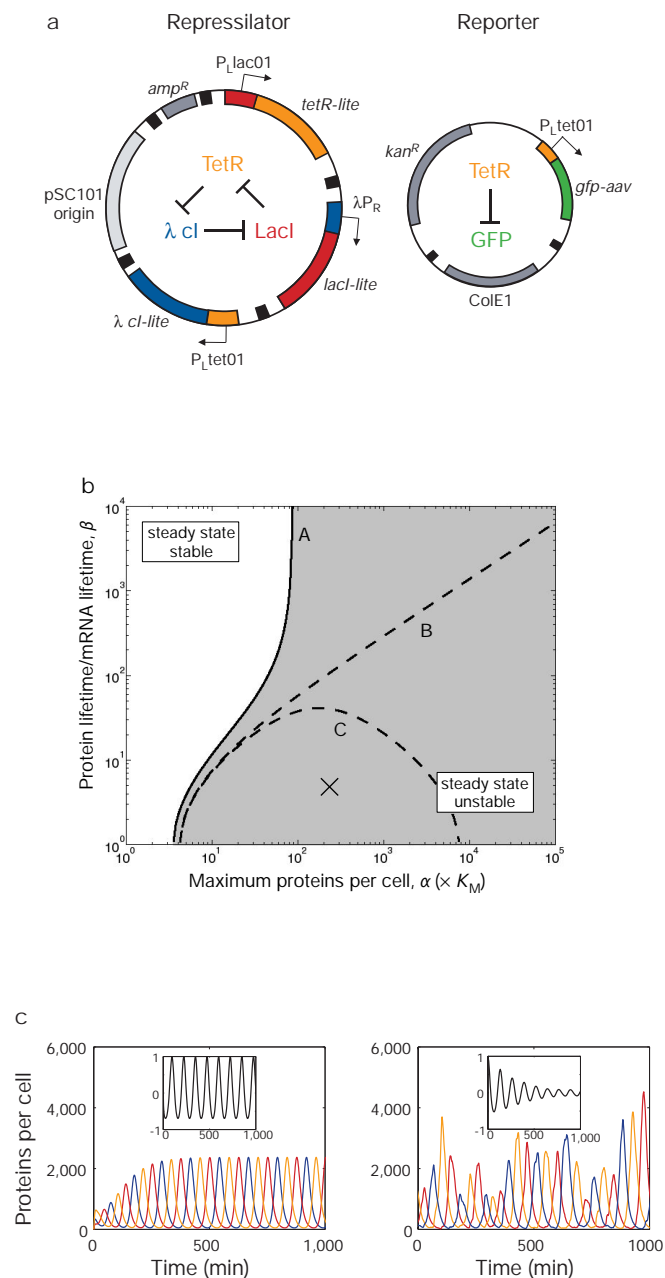


**Figure 1** Construction, design and simulation of the repressor. **a**, The repressor network. The repressor is a cyclic negative-feedback loop composed of three repressor genes and their corresponding promoters, as shown schematically in the centre of the left-hand plasmid. It uses  $P_{lacO1}$  and  $P_{tetO1}$ , which are strong, tightly repressible promoters containing *lac* and *tet* operators, respectively<sup>6</sup>, as well as  $P_R$ , the right promoter from phage  $\lambda$  (see Methods). The stability of the three repressors is reduced by the presence of destruction tags (denoted '*lite*'). The compatible reporter plasmid (right) expresses an intermediate-stability GFP variant<sup>11</sup> (*gfp-aav*). In both plasmids, transcriptional units are isolated from neighbouring regions by T1 terminators from the *E. coli rrnB* operon (black boxes). **b**, Stability diagram for a continuous symmetric repressor model (Box 1). The parameter space is divided into two regions in which the steady state is stable (top left) or unstable (bottom right). Curves A, B and C mark the boundaries between the two regions for different parameter values: A,  $n = 2.1$ ,  $\alpha_0 = 0$ ; B,  $n = 2$ ,  $\alpha_0 = 0$ ; C,  $n = 2$ ,  $\alpha_0/\alpha = 10^{-3}$ . The unstable region (A), which includes unstable regions (B) and (C), is shaded. **c**, Oscillations in the levels of the three repressor proteins, as obtained by numerical integration. Left, a set of typical parameter values, marked by the 'X' in **b**, were used to solve the continuous model. Right, a similar set of parameters was used to solve a stochastic version of the model (Box 1). Colour coding is as in **a**. Insets show the normalized autocorrelation function of the first repressor species.

30 °C. At least 100 individual cell lineages in each of three micro-colonies were tracked manually, and their fluorescence intensity was quantified.

The timecourse of the fluorescence of one such cell is shown in Fig. 2. Temporal oscillations (in this case superimposed on an overall increase in fluorescence) occur with a period of around 150 minutes, roughly threefold longer than the typical cell-division time. The amplitude of oscillations is large compared with baseline levels of GFP fluorescence. At least 40% of cells were found to exhibit oscillatory behaviour in each of the three movies, as determined by a Fourier analysis criterion (see Methods). The range of periods, as estimated by the distribution of peak-to-peak intervals, is  $160 \pm 40$  min (mean  $\pm$  s.d.,  $n = 63$ ). After septation, GFP levels in the two sibling cells often remained correlated with one another for long periods of time (Fig. 3a–c). Based on the analysis of 179 septation events in the 3 movies, we measured an average half-time for sibling decorrelation of  $95 \pm 10$  min, which is longer than the typical cell-division times of 50–70 min under these conditions. This indicates that the state of the network is transmitted to the progeny cells, despite a strong noise component. We observed significant variations in the period and amplitude of the oscillator output both from cell to cell (Fig. 3d), and over time in a single cell and its descendants (Fig. 3a–c). In some individuals, periods were omitted or phase delayed in one cell relative to its sibling (Fig. 3a, c).

Recent theoretical work has shown that stochastic effects may be responsible for noisy operation in natural gene-expression networks<sup>12</sup>. Simulations of the repressor that take into account the stochastic nature of reaction events and discreteness of network components also exhibit significant variability, reducing the correlation time for oscillations from infinity (in the continuous model) to about two periods (Box 1, Fig. 1c, insets). In general, we would like to distinguish such stochastic effects from possible intrinsically complex dynamics (such as intermittence or chaotic behaviour). Further studies are needed to identify and characterize the sources of fluctuations in the repressor and other designed networks. In particular, longer experiments performed under chemostatic conditions should enable more complete statistical characterization of

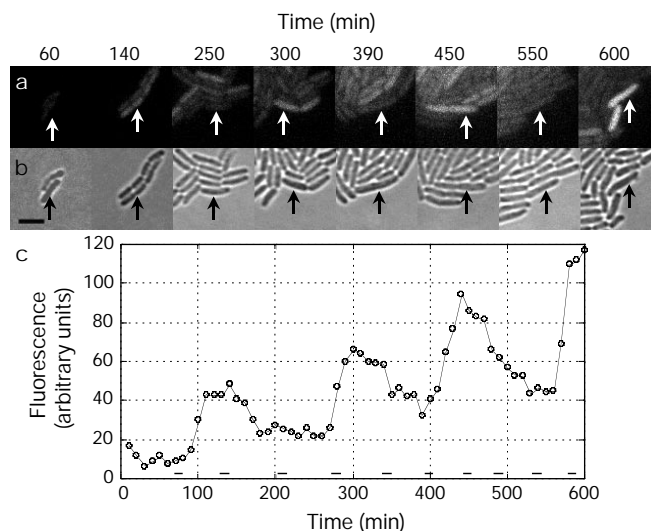


**Figure 2** Repression in living bacteria. **a**, **b**, The growth and timecourse of GFP expression for a single cell of *E. coli* host strain MC4100 containing the repressor plasmids (Fig. 1a). Snapshots of a growing microcolony were taken periodically both in fluorescence (**a**) and bright-field (**b**). **c**, The pictures in **a** and **b** correspond to peaks and troughs in the timecourse of GFP fluorescence density of the selected cell. Scale bar, 4  $\mu$ m. Bars at the bottom of **c** indicate the timing of septation events, as estimated from bright-field images.

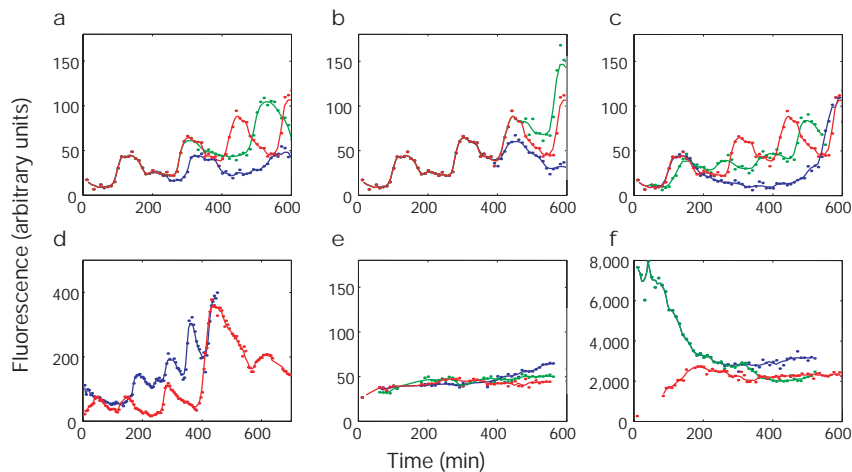


**Figure 3** Examples of oscillatory behaviour and of negative controls. **a–c**, Comparison of the repressilator dynamics exhibited by sibling cells. In each case, the fluorescence timecourse of the cell depicted in Fig. 2 is redrawn in red as a reference, and two of its siblings are shown in blue and green. **a**, Siblings exhibiting post-septation phase delays relative to the reference cell. **b**, Examples where phase is approximately maintained but amplitude varies significantly after division. **c**, Examples of reduced period (green) and

long delay (blue). **d**, Two other examples of oscillatory cells from data obtained in different experiments, under conditions similar to those of **a–c**. There is a large variability in period and amplitude of oscillations. **e, f**, Examples of negative control experiments. **e**, Cells containing the repressilator were disrupted by growth in media containing 50  $\mu\text{M}$  IPTG. **f**, Cells containing only the reporter plasmid.

Box 1

**Network design**

Design of the repressilator started with a simple mathematical model of transcriptional regulation. We did not set out to describe precisely the behaviour of the system, as not enough is known about the molecular interactions inside the cell to make such a description realistic. Instead, we hoped to identify possible classes of dynamic behaviour and determine which experimental parameters should be adjusted to obtain sustained oscillations.

**Deterministic, continuous approximation**

Three repressor-protein concentrations,  $p_i$ , and their corresponding mRNA concentrations,  $m_i$  (where  $i$  is *lacI*, *tetR* or *cl*) were treated as continuous dynamical variables. Each of these six molecular species participates in transcription, translation and degradation reactions. Here we consider only the symmetrical case in which all three repressors are identical except for their DNA-binding specificities. The kinetics of the system are determined by six coupled first-order differential equations:

$$\frac{dm_i}{dt} = -m_i + \frac{\alpha}{(1+p_i^n)} + \alpha_0 \quad (i = lacI, tetR, cl)$$

$$\frac{dp_i}{dt} = -\beta(p_i - m_i) \quad (j = cl, lacI, tetR)$$

where the number of protein copies per cell produced from a given promoter type during continuous growth is  $\alpha_0$  in the presence of saturating amounts of repressor (owing to the ‘leakiness’ of the promoter), and  $\alpha + \alpha_0$  in its absence;  $\beta$  denotes the ratio of the protein decay rate to the mRNA decay rate; and  $n$  is a Hill coefficient. Time is rescaled in units of the mRNA lifetime; protein concentrations are written in units of  $K_M$ , the number of repressors necessary to half-maximally repress a promoter; and mRNA concentrations are rescaled by their translation efficiency, the average number of proteins produced per mRNA molecule. The numerical solution of the model shown in Fig. 1c used the following parameter values: promoter strength,  $5 \times 10^{-4}$  (repressed) to 0.5 (fully induced) transcripts per s; average translation efficiency, 20 proteins per transcript, Hill coefficient,  $n = 2$ ; protein half-life, 10 min; mRNA half-life, 2 min;  $K_M$ , 40 monomers per cell.

This system of equations has a unique steady state, which becomes unstable when  $\frac{(\beta + 1)^2}{\beta} < \frac{3X^2}{4 + 2X}$ , where  $X \equiv -\frac{\alpha n p^{n-1}}{(1+p^n)^2}$  and  $p$  is the solution to  $p = \frac{\alpha}{1+p^n} + \alpha_0$ . The boundary between the stable and

unstable domains can therefore be plotted (Fig. 1b). The unstable domain becomes much larger when the Hill coefficient increases, removing any limitation on  $\beta$  for sufficiently large  $\alpha$  (compare curve B, for which  $n = 2$ , to curve A, for which  $n = 2.1$ ). The effect of leakiness,  $\alpha_0$ , can be seen by plotting the stability boundary for a constant ratio of  $\alpha_0/\alpha$ , as in curve C. When  $\alpha_0$  becomes comparable to  $K_M$  (1 in our units), the unstable domain shrinks (compare curve B, for which  $\alpha_0 = 0$ , to curve C, for which  $\alpha_0/\alpha = 10^{-3}$ ). Similar analysis of the stability of the steady state can be performed for generalized models of cyclic transcriptional feedback loops. The simplest such networks supporting limit-cycle oscillations are those containing a single repressor and a single activator, or an odd number of repressors exceeding 3. In general, the period of oscillations in such networks is determined mainly by the protein stability<sup>16</sup>. More detailed calculations, with non-Hill-function repression curves, or using thermodynamic binding energies to predict equilibrium operator occupancies, and taking repressor dimerization into account, yield similar stability results<sup>19</sup>. It is possible that, in addition to simple oscillations, this and more realistic models may exhibit other complex types of dynamic behaviour.

**Stochastic, discrete approximation**

The preceding analysis neglects the discrete nature of the molecular components and the stochastic character of their interactions, however. Such effects are believed to be important in biochemical and genetic networks<sup>12</sup>. We therefore adapted the above equations to perform stochastic simulations, as described<sup>20</sup>. To obtain cooperativity in repression analogous to the continuous case, we assumed the presence of two operator sites on each promoter and the following reactions: binding of proteins to each operator site ( $1 \text{ nM}^{-1} \text{ s}^{-1}$ ); unbinding of protein from the first-occupied ( $224 \text{ s}^{-1}$ ) and the second-occupied ( $9 \text{ s}^{-1}$ ) operator; transcription from occupied ( $5 \times 10^{-4} \text{ s}^{-1}$ ) and from unoccupied ( $0.5 \text{ s}^{-1}$ ) promoters; translation ( $0.167 \text{ mRNA}^{-1} \text{ s}^{-1}$ ); protein decay ( $10 \text{ min half-life}$ ); and mRNA decay ( $2 \text{ min half-life}$ ). These parameters were chosen to correspond as closely as possible to the continuous model described above, assuming that 1 molecule per cell corresponds to a concentration of  $\sim 1 \text{ nM}$ . Oscillations persist for these parameter values (Fig. 1c) but with a large variability, resulting in a finite autocorrelation time (compare insets in Fig. 1c).

the noisy repressilator dynamics. In addition, varying the host species and genetic background would allow us to check for, and minimize, spurious interactions with endogenous cellular sub-systems, and to investigate how the network is embedded in the cell. For instance, in the repressilator network, the cell-division cycle does not seem to be coupled with the repressilator, as the timing of oscillations is uncorrelated with cell septation events (Fig. 2). However, entry into the stationary phase causes the repressilator to halt, indicating that the network is coupled to the global regulation of cell growth.

The levels of many cellular components vary over time in growing cells, and even strains that constitutively express GFP exhibit significant heterogeneity, so we performed several control experiments to check that the observed oscillations are indeed due to the repressilator (Fig. 3e, f). These included deliberate disruption of the network (by adding sufficient IPTG to interfere with LacI) and observation of GFP expression in the absence of the repressilator (from plasmids with different promoters and origins of replication).

Our results show that it is possible to design and construct an artificial genetic network with new functional properties from generic components that naturally occur in other contexts. Such work is analogous to the rational design of functional proteins from well-characterized motifs<sup>13</sup>. Further characterization of components and alteration of network connectivity may reveal general features of this and related networks, and provide a basis for improved design and possible use in biotechnological applications. Moreover, comparing designed networks with their evolved counterparts may also help us to understand the 'design principles' underlying the latter. For instance, circadian clocks are found in many organisms, including cyanobacteria in which the cell-division time may be shorter than the period<sup>14–15</sup>. However, the reliable performance of such circadian oscillators can be contrasted with the noisy, variable behaviour of the repressilator. Instead of three repressors, it seems that circadian oscillators use both positive and negative control elements. Does this design lead to improved reliability? Recent theoretical analysis suggests that, in the presence of interactions between positive and negative control elements that lead to bistable, hysteretic behaviour, an oscillating circuit does indeed exhibit high noise-resistance<sup>16</sup>. It would be interesting to see whether one could build an artificial analogue of the circadian clock, and, if so, whether such an analogue would display the noise resistance and temperature compensation of its natural counterpart. □

## Methods

### Network construction

The three repressors (*lacI*, *tetR* and *cI*), the  $\lambda$  promoter  $P_R$  and the unstable variants of *gfp*<sup>11</sup> were all cloned by the polymerase chain reaction (PCR) and verified by sequencing. In the case of *lacI*, the GTG start codon was changed to ATG with the 5' primer. 3' PCR primers were used to add the coding sequence for the 11-amino-acid *ssrA* tag to the three repressors<sup>8</sup>. Tagging of full-length  $\lambda$  repressor, as well as *lacI* and *tetR*, resulted in functional proteins that required increased induction to achieve full repression, consistent with decreased stability. Promoter sequences  $P_{lacO1}$  and  $P_{tetO1}$  were obtained from pZE21-MCSI and pZE12-luc<sup>6</sup>. The repressilator plasmid was constructed in three successive cloning steps from intermediate plasmids containing the three transcriptional units. The reporter plasmid was constructed by cloning the GFPaav variant<sup>11</sup>, which has a half-life of around 90 min, into pZE21-MCSI (ref. 6). The finite rate at which GFP is oxidized to its fluorescent form<sup>17</sup> and its relatively long half-life limit our ability to observe fast dynamic phenomena. The presence of additional *tet* operators on the reporter plasmid constitutes a perturbation to the single-plasmid repressilator network by titrating out repressors<sup>18</sup>.

### Data acquisition and analysis

Cells of *E. coli lac*<sup>-</sup> strain MC4100 (unless otherwise specified) transformed with appropriate plasmids were grown in minimal media (7.6 mM [NH<sub>4</sub>]<sub>2</sub>SO<sub>4</sub>, 2 mM MgSO<sub>4</sub>, 30  $\mu$ M FeSO<sub>4</sub>, 1 mM EDTA, 60 mM potassium phosphate, pH 6.8) supplemented with 0.5% glycerol, 0.1% casamino acids and appropriate antibiotics (20  $\mu$ g ml<sup>-1</sup> kanamycin or 20  $\mu$ g ml<sup>-1</sup> ampicillin), when needed. Time-lapse microscopy was conducted on a Zeiss Axiovert 135TV microscope equipped with a 512  $\times$  512-pixel cooled CCD camera (Princeton Instruments). Cultures were grown for at least 10 hours to optical density of 0.1 at 600 nm, diluted into fresh media, spotted between a coverslip and 1 ml of liquid 2%

SeaPlaque low-melt agarose (FMC) in media, and sealed. The temperature of the samples was maintained at 30–32 °C by using Peltier devices (Melcor). Bright-field (0.1 s) and epifluorescence (0.05–0.5 s) exposures were taken periodically (every 5 or 10 min). All light sources (standard 100 W Hg and halogen lamps) were shuttered between exposures. Images were flat-field corrected with custom software. For the synchronization experiment, overnight cultures were diluted back 1:100 in media containing 100  $\mu$ M IPTG, grown to mid-log, washed several times, and diluted again and grown in 96-well plates at 30 with shaking in a Wallac Victor 2 plate reader, while fluorescence and absorbance measurements were taken every 5 min.

For analysis, cells were selected from the final frames of bright-field movies, without regard to their fluorescence signals, and tracked manually backward in time until the first frame. At each time point, the cell position was identified on the bright-field image, and fluorescence intensity data were averaged over a 28-pixel region, similar in size to the cell diameter, in the corresponding location on the fluorescence image. A fast Fourier transform was applied to the temporal fluorescence signal from each analysed cell lineage and divided by the transform of a decaying exponential with a time constant of 90 min, the measured lifetime of GFPaav. Power spectra exhibiting peaks of more than four times the background at frequencies of 0.2–0.5 per hour were classified as oscillatory (the choice of threshold alters the fraction of oscillatory cells defined by this criterion). The sibling 'decorrelation' half-time was defined as the time necessary for the quantity  $|I_1(t) - I_2(t)| / (I_1(t) + I_2(t))$ , averaged over pairs of daughter cells, to reach half of its asymptotic value. Here,  $I_1(t)$  and  $I_2(t)$  denote the fluorescence intensities of the two sibling cells at times,  $t$ , starting from the moment of septation ( $\pm 10$  min). In this analysis, only cells judged to be oscillatory by the Fourier criterion were considered.

Various negative control experiments were performed. First, 50  $\mu$ M IPTG was added to the media to disrupt the functioning of the network (Fig. 3c). Second, we used a version of the repressilator plasmid lacking all but the *tetR* transcriptional unit (in *lacI*<sup>fl</sup> strain JM109). We thus varied GFP expression of the reporter plasmid by controlling TetR levels with 0–20  $\mu$ M IPTG. Third, we examined cells containing only the reporter plasmid (Fig. 3f). Fourth, we measured GFP expression from reporter plasmids modified in several ways either by replacing the  $P_{tetO1}$  promoter with each of the two other promoters, and *gfp-aav* with *gfp-lite*<sup>11</sup> (the suffix 'lite' indicates the presence of a C-terminal *ssrA* tag), or by replacing the ColE1 origin of replication with the lower-copy pSC101 origin normally used on the repressilator plasmid. In none of these control experiments did we observe oscillations similar to those produced by the repressilator.

Received 6 July; accepted 9 November 1999.

1. Bray, D. Protein molecules as computational elements in living cells. *Nature* **376**, 307–312 (1995).
2. Koshland, D. E. Jr The era of pathway quantification. *Science* **280**, 852–853 (1998).
3. Winfree, A. T. *The Geometry of Biological Time* (Springer, Berlin, 1990).
4. Goldbeter, A. *Biochemical Oscillations and Cellular Rhythms* (Cambridge Univ. Press, 1996).
5. Thomas, R. & D'Ari, R. *Biological Feedback* (CRC Press, Boca Raton, 1990).
6. Lutz, R. & Bujard, H. Independent and tight regulation of transcriptional units in *Escherichia coli* via the LacR/O, the TetR/O and AraC/11-12 regulatory elements. *Nucleic Acids Res.* **25**, 1203–1210 (1997).
7. Kushner, S. R. in *Escherichia Coli and Salmonella: Cellular and Molecular Biology* (ed. Neidhardt, F. C.) (ASM, Washington DC, 1996).
8. Keiler, K. C., Waller, P. R. & Sauer, R. T. Role of a peptide tagging system in degradation of proteins synthesized from damaged messenger RNA. *Science* **271**, 990–993 (1996).
9. Gottesman, S., Roche, E., Zhou, Y. & Sauer, R. T. The ClpXP and ClpAP proteases degrade proteins with carboxy-terminal peptide tails added by the SsrA-tagging system. *Genes Dev.* **12**, 1338–1347 (1998).
10. Herman, C., Thevenet, D., Bouloc, P., Walker, G. C. & D'Ari, R. Degradation of carboxy-terminal-tagged cytoplasmic proteins by the *Escherichia coli* protease HflB (FtsH). *Genes Dev.* **12**, 1348–1355 (1998).
11. Andersen, J. B. *et al.* New unstable variants of green fluorescent protein for studies of transient gene expression in bacteria. *Appl. Environ. Microbiol.* **64**, 2240–2246 (1998).
12. McAdams, H. H. & Arkin, A. It's a noisy business! Genetic regulation at the nanomolar scale. *Trends Genet.* **15**, 65–69 (1999).
13. Bryson, J. W. *et al.* Protein design: a hierarchic approach. *Science* **270**, 935–941 (1995).
14. Dunlap, J. C. Molecular bases for circadian clocks. *Cell* **96**, 271–290 (1999).
15. Kondo, T. *et al.* Circadian rhythms in rapidly dividing cyanobacteria. *Science* **275**, 224–227 (1997).
16. Barkai, N. & Leibler, S. Circadian clocks limited by noise. *Nature* (submitted????). (Eds to update)
17. Tsien, R. Y. The green fluorescent protein. *Annu. Rev. Biochem.* **67**, 509–544 (1998).
18. Glascock, C. B. & Weickert, M. J. Using chromosomal lacQ1 to control expression of genes on high-copy-number plasmids in *Escherichia coli*. *Gene* **223**, 221–231 (1998).
19. Elowitz, M. B. *Transport, Assembly, and Dynamics in Systems of Interacting Proteins*. Thesis, Princeton Univ., Princeton (1999).
20. Gillespie, D. T. Exact stochastic simulation of coupled chemical reactions. *J. Phys. Chem.* **81**, 2340–2361 (1977).

### Acknowledgements

We thank H. Bujard, S. Freundlieb, A. Hochschild, R. Lutz and C. Sternberg for plasmids and advice; U. Alon, N. Barkai, P. Cluzel, L. Frisen, C. Guet, T. Hyman, R. Kishony, A. Jaedicke, P. Lopez, F. Nédélec, S. Pichler, R. Kishony, T. Silhavy, T. Surrey, J. Vilar, C. Wiggins and E. Winfree for discussions; M. Surette for advice and encouragement; L. Hartwell and C. Weitz for comments on the manuscript; and F. Kafatos and E. Karsenti for hospitality and support at the European Molecular Biology Laboratory (EMBL), where part of this work was done. This work was partly supported by the US National Institutes of Health and the von Humboldt Foundation.

Correspondence and requests for materials should be addressed to M.B.E. (e-mail: melowitz@princeton.edu).